Accepted Manuscript

Nonlinear optical absorption of SnX_2 (X = S, Se) semiconductor nanosheets

Jia-Jing Wu, You-Rong Tao, Xing-Cai Wu, Yuan Chun

PII: S0925-8388(17)31376-2

DOI: 10.1016/j.jallcom.2017.04.177

Reference: JALCOM 41581

To appear in: *Journal of Alloys and Compounds*

Received Date: 5 December 2016

Revised Date: 5 April 2017

Accepted Date: 16 April 2017

Please cite this article as: J.-J. Wu, Y.-R. Tao, X.-C. Wu, Y. Chun, Nonlinear optical absorption of SnX_2 (X = S, Se) semiconductor nanosheets, *Journal of Alloys and Compounds* (2017), doi: 10.1016/j.jallcom.2017.04.177.

Nonlinear Optical Absorption of SnX_2 (X=S, Se) Semiconductor Nanosheets

Jia-Jing Wu, You-Rong Tao, Xing-Cai Wu*, and Yuan Chun*

The nonlinear absorption performance of SnX_2 (X= S, Se) was measured by Z-Scan technique at nanosecond pulse and picosecond pulse, the results show that SnS_2 nanosheets have excellent optical limiting property and optical limiting threshold F_{th} is about 0.23 J/cm^2. However, $SnSe_2$ nanosheets exhibit saturable absorption behavior.

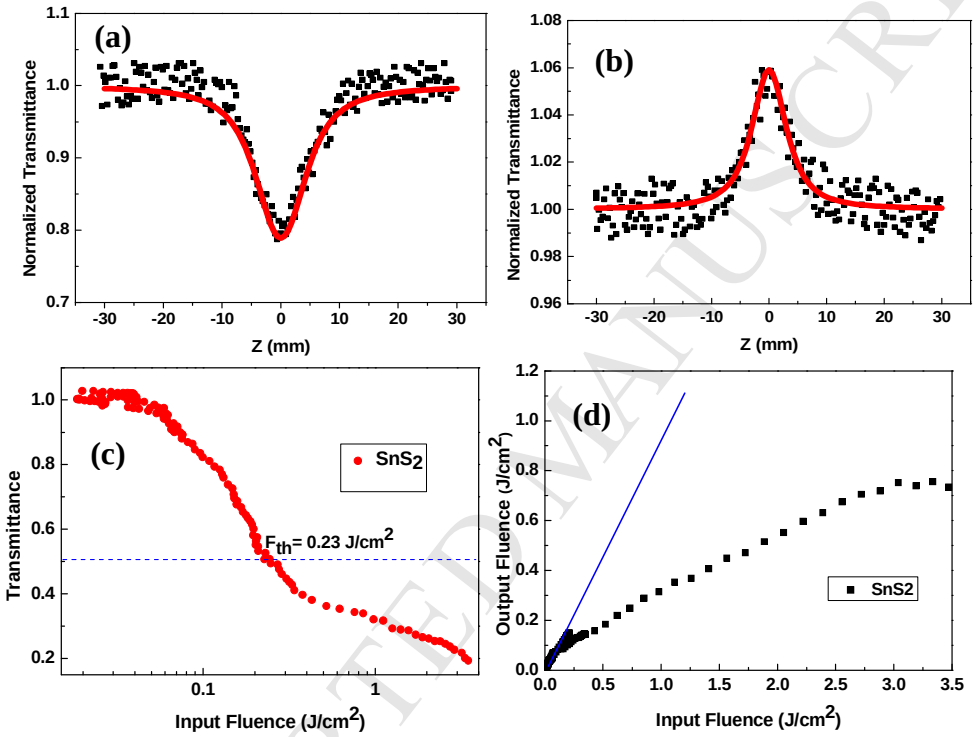

Nonlinear optical absorption of SnX_2 (X=S, Se) semiconductor nanosheets

Jia-Jing Wu, You-Rong Tao, Xing-Cai Wu*, Yuan Chun*

Key Laboratory of Mesoscopic Chemistry of MOE, and State Key Laboratory of Coordination Chemistry, and School of Chemistry and Chemical Engineering, Nanjing University, Nanjing 210093, China.

Abstract

Tin-based dichalcogenides such as SnS_2 and $SnSe_2$ have attracted wide attention due to their significant potential for the next-generation optoelectronic and photonic devices in nanotechnology. We investigate the nonlinear absorption of SnS_2 and $SnSe_2$ nanosheets using the Z-scan technique with nanosecond pulse and picosecond at 532 nm for the first time. Z-scan measurement reveals that SnS_2 nanosheets dispersions exhibit reverse saturable absorption (RSA) behavior under different pulses, which is in contrast to the saturable absorption (SA) observed in the $SnSe_2$ naosheets dispersions resulted from different band gaps. The nonlinear absorption coefficient (β) and the figures of merit (FOM) of SnS_2 dispersed in ethanol with linear transmittances of 0.75 at input energy of 6.16 μJ in the nanosecond regime are 12.78×10^{-10} m/W and 8.71×10^{-11} esu·cm, respectively. As for $SnSe_2$ nanosheet dispersions, β and FOM are -12.58×10^{-10} m/W and 11.98×10^{-11} esu·cm at the same input energy, respectively. The RSA behavior coupled to the smaller optical limiting threshold F_{th} (0.23 J/cm^2) proves SnS_2 a promising 2D material for protecting sensitive optical components or eyes from laser-induced damage. The SA performance indicates $SnSe_2$ nanosheets prospective candidates for high-performance nanoscale nanophotonic devices like optical switches.

Keywords: Tin-based dichalcogenides, Nanosheet, Nonlinear absorption, Optical limiting.

*Corresponding author. Fax: +86 25 83317761.

E-mail: wuxingca@nju.edu.cn (X. C. Wu); ychun@nju.edu.cn (Y. Chun).

1. Introduction

Layered two-dimensional (2D) semiconductor nanostructures such as graphene, black phosphorus (BP) and metal Dichalcogenides (MDCs) have extensively been used as building blocks in many electronic, photonic and optoelectronic devices, including field-effect transistors (FETs), photodetectors, saturable absorbers, optical switches and optical limiters[1–9]. Recently, nanophotonic devices based on transition metal chalcogenides (MX_2, M =Mo and W; X=S, Se and Te) have attracted specially increasing interest due to tunable bandgaps and large specific surface area. For example, saturable absorbers and Q-Switcher based on 2D nanostructure like MoS_2, WS_2 have been extensively investigated [10–12]. Besides, the nonlinear optical (NLO) performance of BP nanosheets has been intriguing intensive attention [13,14]. However, it is important to obtain earth-abundant and environment-friendly materials with NLO properties.

SnS_2 and $SnSe_2$ as important IVA-VIA semiconductors have tunable bandgaps of 2.35 eV and 1.1 eV, respectively, with a layered CdI_2-type sandwiched structure where Sn layer located between two S or Se layers [15, 16]. The nontoxicity and low cost ensure them obvious advantages in electronics and optoelectronics. Presently, they have been fabricated into photodetectors [15–17]. Here we study the NLO properties of SnS_2 and $SnSe_2$ nanosheet dispersions, and find their good optical limit effect of SnS_2 nanosheets. To our knowledge, it is the first report.

2. Experimental Material Preparation and Characterization

2. 1. Synthesis

The SnS_2 Nanosheet microspheres and $SnSe_2$ hexagonal nanosheets were synthesized by a facile ethanol thermal and hydrothermal method, respectively [2, 18].

SnS_2 Nanosheet: 0.005 mol. $SnCl_4•5H_2O$ (C. P.) and 0.02 mol. thioacetamide (A. R.) were added into a 100 ml beaker, then 40 ml ethanol was added, next the solution was stirred for about 30 min. Followed by, the mixture was put into Teflon-lined stainless steel autoclave, and heated at 180℃ for 24 h in a drying cabinet. Afterwards the cabinet was cooled down to room temperature naturally. The yellow product was collected by centrifugation, alternately washed with deionized water and absolute ethanol, and then dried at 60 ℃ for 2 h.

$SnSe_2$ hexagonal nanosheets: 1.128 g $SnCl_2•2H_2O$ and 1.1096 g SeO_2 were dispersed in distilled water (40 ml) by stirring magnetically for 5 min and sonication for 10 min to form a homogeneous solution, and then the solution was transferred into a Teflon-lined stainless steel autoclave. Afterwards, 2 ml hydrazine hydrate ($N_2H_4•H_2O$) was added into the reactants, followed by the reaction temperature raised to 180℃ and maintained for 24 h. At last, the obtained product was collected by centrifugation, alternately washed with water and ethanol, and dried in a drying cabinet at 60 ℃ for 2 h.

SnX_2 dispersions: Initial SnX_2 dispersions (0.1 mg/mL) were produced by sonicating for 2 h using a 120 W ultrasonic cleaner, afterwards centrifugation at 3000 rpm for 10 min to remove large aggregates. The digital photograph of SnX_2 dispersion was shown in Figure S1.

2. 2. *Characterization and Measurements*

The characterization of the as-prepared products was characterized by X-ray diffraction (XRD, Shimadzu XRD-6000 with graphite monochromatized Cu Kα1 radiation), a field-emission scanning electron microscope (FE-SEM, Hitachi S-4800), a high-resolution transmission electron microscope (HRTEM, JEM-2100) and Raman Spectroscopy (LabRAM Aramis).

3. **Results and discussion**

Fig. 1(a) and (b) reveal X-ray diffraction (XRD) patterns of as-synthesized products. In Fig. 1(a), all the peaks can be properly indexed to hexagonal SnS_2 (X'pert highscore plus reference code: 00－023－

0677) without any detectable crystalline impurity phase. In Fig. 1b, the XRD pattern shows that the as-prepared products are hexagonal $SnSe_2$ (X'pert highscore plus reference code: 01－089－319) without other phases. The four predominant peaks at 2θ =14.51°, 30.68°, 40.05°, and 47.81° correspond to the (001), (011), (012), and (110) of hexagonal $SnSe_2$, respectively.

The field-emission scanning electron microscopy (FESEM) in Fig. 2(a) reveals the formation of microspheres flower-like nanostructure with diameter of about 2–5 μm, Fig. 2(b) shows the high-magnification SEM image of microspheres of the self-assembled nanosheets with the thickness less than 30 nm. The SEM image in Fig. 2(c) reveals the formation of hexagonal nanosheets with the length of 0.5–5 μm, Fig. 2(d) is a high-magnification SEM image of $SnSe_2$ hexagonal nanosheets with thickness of 30–40 nm.

Fig. 3(a) contains a typical transmission electron microscopic (TEM) image of an approximate microsphere consists of SnS_2 nanosheets with diameters of about 65 nm. Figure 3(b) is the TEM image of the edge of SnS_2 microsphere, and corresponding selected area electron diffraction (SAED) pattern is shown in Fig. 3(c). Fig. 3(d) presents a high-resolution TEM (HRTEM) image, observing an lattice spacing of 0.27 nm, which corresponds to the (101) plane of SnS_2. Fig. 3(e) displays TEM image of bulk hexagonal $SnSe_2$, showing a typical plate-like morphology with lateral size of about 0.4–2μm, while the nearly transparent feature reveals the ultrathin thickness. Fig. 3(f) shows a large-area 2D hexagonal sheet-like structure with a length larger than 600 nm, and Fig. 3(g) is its SAED pattern. The HRTEM image of $SnSe_2$ nanosheet [Fig. 3(h)] reveals that the d-spacing is 0.33 nm, corresponding to the (100) plane of hexagonal $SnSe_2$.

Raman Spectroscopy in Fig. 4(a) confirms that as-prepared products are indeed pure SnS_2 nanosheets with a strong Raman peak at 312.6 cm^{-1} assigned to A_{1g} mode [19]. Here weak intra-layer E_g mode peak located at 200–205 cm^{-1} cannot be observed, because of the sensitivity limitation of the sensor or the selection rules of scattering geometry [20], demonstrating the as-synthesized SnS_2 nanosheets belong to 2H-SnS_2 instead of 4H-SnS_2. In Fig. 4(b), two characteristic peaks can be observed in the measurement range from 100 to 300 cm^{-1} under the 532 nm laser excitations. The one at 116.2cm^{-1} is assigned to the in-

plane (E_g) mode of the Se–Sn–Se lattice, and the other at 184.4 cm^{-1} assigned to the out-of-plane (A_{1g}) mode [21].

An ultraviolet-visible (UV-vis) absorption spectrum of SnS_2 dispersions is shown in Fig. 4(c), the two characteristic absorption peaks at 268 nm (4.63 eV) and 425 nm (2.92 eV). Fig. 4(d) is the UV-vis spectrum of $SnSe_2$ dispersions, revealing that $SnSe_2$ nanosheeets have a broad absorption band from 250–900 nm. In UV region, two obvious absorption peaks appear at 261 nm (4.75 eV) and 345 nm (3.59 eV). The two main peaks can be assigned to transition from the crystal field split anion p_z- and p_{xy}-like levels, respectively, into anion and cation s- and p-like levels, respectively [22，23].

The NLO properties of SnS_2 nanosheets and $SnSe_2$ nanosheets are investigated using an open aperture Z-scan with 6.5 ns Nd:YAG pulsed Q-switched frequency-double laser operating at 532 nm (2.33 eV) with a repetition rate of 10 Hz. The radius of the beam waist (w_0) is 40 μm, and the confocal parameter (z_0) is 9.6 mm, much greater than the thickness of the sample cuvette (2 mm), which is a key parameter for Z-scan technique. The propagation direction (Z-axis) of laser pulses passed through sample which is installed on a moving platform that is controlled by a computer. The Z-scan experimental setup [Fig. S(2)] is parallel to our previous measurement of ZrS_3 dispersions [24].

Fig. 5(a–d) shows the NLO response of SnS_2 nanosheets with the linear transmittance (T_s) of 0.75 excited by 532 nm laser pulses at different input energy from 1.37 μJ to 51.6 μJ. Fig. 5(a), the normalized transmittance gradually increases with the increase of laser intensity ($z \rightarrow 0$), shows a symmetrical peak with respect to the focus ($z=0$) at low input energy of 1.37 μJ. This nonlinear absorption (NLA) is typical saturable absorption (SA) process originating from one-photo absorption. When the input energy increase to 6.16 μJ, the normalized transmittance decrease as laser intensity ($z \rightarrow 0$) increases, and the normalized transmittance curve appears an obvious valley at the focus point ($z = 0$), and the shape of curve is symmetrical with respect to the focus point, indicating the reverse saturable absorption (RSA) behavior in the SnS_2 dispersions begin to dominate NLA mechanism.With the increase of the input energy, the RSA response of SnS_2 nanosheets increases. The variation of the normalized transmittance at the focus (T_a) as a

function of the input energy is shown in Fig. 5(e). The transmittance decreases with increase in input energy, indicating the dependence of NLO response on the input energy. At the input energy of 6.16 μJ, the transmittance is 0.76, the T_a value decreases to 0.376 at the energy of 45.46 μJ. That is to say, the higher input energy corresponds to the deeper valley at focus. When the input energy is continually increased to be 48.58 and 51.6 μJ, the T_a values have not obvious variation.

Open aperature Z-scan data were fitted by the nonlinear propagation equation [25]:

$$dI/dz' = -\alpha(I)I$$

Where α(I) is absorption coefficient, including linear and nonlinear absorption parts. From the fitting curves [solid lines in Fig. 5(a–d)], the experimental data were fitted perfectly based on the nonlinear absorption model. The fitting open aperture (OA) curves are shown in Fig. 5(f). The nonlinear absorption coefficient for SnS_2 dispersions at different input energy is shown in Fig. 5(g), and the nonlinear absorption coefficient is 12.78×10^{-10} m/W at 6.16 μJ, decreasing monotonically to 3.91×10^{-10} m/W at 53.75 μJ. The imaginary ($Im\chi^{(3)}$) part of the three-order NLO susceptibility can be calculated by nonlinear absorption coefficient with the equation $Im\chi^{(3)} = 10^{-7}c\lambda n_0^2\beta/96\pi^2$, here c represents the speed of light, n_0 represents the refractive index. The figure of merit (FOM) is defined as FOM =$|Im\chi^{(3)}/\alpha_0|$. The $Im\chi^{(3)}$ and FOM of SnS_2 nanosheets decreases gradually with increase of input energy as shown in Fig. 5(h).

The nonlinear optical absorption properties of $SnSe_2$ hexagonal nanosheets are shown Fig. 6(a) and 6(b). The normalized transmittance curves have an obvious peak at the laser focus at low input energy (2.2 μJ and 6.16 μJ), showing the transmittance of the sample increases with the increasing input laser intensity, indicating that it should have stronger SA behaviour induced by one-photon absorption. When the input energy continues to increase, the transmittance also decreases with the laser intensity increase. This tendency is similar to SnS_2 nanosheets. Fig. 6(c) displays the OA theory curve of SnS_2 nanosheets which reveal the NLA performance of $SnSe_2$ is influenced by the change of input energy. Fig. 6(d) shows the T_a value reduces as the input energy increases. And the nonlinear absorption coefficient of $SnSe_2$ hexagonal nanosheets decreases from 49.8 cm/GW at the input energy of 11.98 μJ to 30.2 cm/GW at 52.06 μJ, as is

shown in Fig. 6(e). The variation of $Im\chi^{(3)}$ and FOM in $SnSe_2$ nanosheets dispersions with input energy is shown in Fig. 6(f).

Generally, the SA at 532 nm (2.33 eV) under low input energy can be ascribed to valence conduction inter-band transition, as the input energy increases, electrons in the valence band can be easily filled the conduction band. Due to the Pauli blocking, the optical absorption reached saturation at a high input energy. Besides, $SnSe_2$ nanosheets with incident photons energy larger than band gap show saturable absorption response, the cause of the free carrier excitation from valence band to conduction band. SnS_2 nanosheets with the band gap near the incident photons energy exhibit RSA behavior, which is attributed to the resonance of TPA near the band edge at 532 nm.

To further investigate the effects of solvent on the NLO performance of SnX_2 nanaosheets, the sample were dispersed in different boiling point solvents including water, ethanol and NMP, the experimental results were shown in Fig. S3 and S4. Fig.S3 exhibits the RSA response of SnS_2 in the different solvents in the nanosecond regime at the same input energy of 10 μJ, and the NLA coefficients were 10.16×10^{-10} m/W, 7.82×10^{-10} m/W, and 4.53×10^{-10} m/W for ethanol, water and NMP, respectively. Fig.S4 shows the SA of $SnSe_2$ in different solvents in nanosecond regime at the same input energy of 8.47 μJ, and the nonlinear absorption coefficients were -2.59×10^{-10} m/W, -4.03×10^{-10} m/W, and -8.62×10^{-10} m/W for ethanol, water, and NMP, respectively. Therefore, NLO of SnX_2 was influenced by solvent, which may be attributed to the linear absorbance and the Lorentz-Lorenz local field correction factors [26, 27]. Besides, we measure the NLO of different solvents, as is shown in Fig. S5, but we cannot observe obvious NLA response.

Additionally, to eliminate thermal effects on the NLO performance, we applied a 532 nm picosecond laser with the pulse duration of 21 ps. Fig. 7(a) and 7(b) show the NLO response of SnS_2 and $SnSe_2$ dispersions at the input energy of 1.4 μJ, respectively. For the dispersions of SnS_2 the transmittance decreased sharply near the laser focus, indicating a higher absorbance at higher laser intensity, which shows RSA behavior take place in the dispersion. In contrast, the $SnSe_2$ dispersions exhibit an increased transmittance around the zero Z-position, pointing to SA properties. The nonlinear absorption coefficient

obtained from the fitting is 3×10^{-12} m/W for SnS_2 nanosheets and is -3.8×10^{-13} m/W for $SnSe_2$ hexagonal nanosheets.

Table 1 lists the linear and nonlinear parameters of the SnS_2 and $SnSe_2$ nanosheets measured by nanosecond and picosecond Z-scan technique. The results demonstrate that SnS_2 exhibits RSA response and $SnSe_2$ shows SA performance in nanosecond and picosecond regime. Moreover, their nonlinear absorption coefficients have obvious difference at different laser pulses caused by excited state absorption. FOM of SnS_2 and $SnSe_2$ dispersions at nanosecond laser pulse are three and four orders of magnitude larger than that at picosecond pulse, respectively.

To evaluate the NLO performance of the as-synthesized SnS_2 and $SnSe_2$ dispersions, we also summarize the relevant figures of merit reported in literature for other nanomaterials in Table 1, and the experimental conditions are also listed for comparison. The measured FOM values of SnS_2 and $SnSe_2$ is larger than ZrS_3 nanosheets [24], WS_2 [28] and RGO [29], comparable with MoS_2 [30], BP [6], $AgInSe_2$ [31] and Au [32] nanomaterials. Therefore, the eco-friendly SnX_2 compound will be a promising material for photonic device.

According to the results discussed above, SnS_2 nanosheets exhibit excellent reverse saturation absorption property, revealing that it should possess optical limiting (OL) performance. So the OL measurements were performed at excitation wavelength of 532 nm with 21 ps pulsed laser. Fig. 8(a) shows the observed variation of transmittance with the input fluence for SnS_2 nanosheets in ethanol dispersions with linear transmittance of 0.75. It is clear that the transmittance decreases as the input fluence increases. The optical limiting threshold F_{th}, defined as the input fluence at which the transmittance is 50 % of the linear transmittance, was measured about 0.23 J/cm^2 for SnS_2 nanosheets dispersions. The Fth of SnS_2 is far smaller than MoS_2 (11.16 J/cm^2), $MoSe_2$ (7.3 J/cm^2), WS_2 (9.35 J/cm^2), WSe_2 (7.2 J/cm^2) and graphene (15.15 J/cm^2) in previously measured [33]. The plot of output fluence against input fluence for SnS_2 nanosheets is shown in Fig. 8(b). At very low input fluence, the output fluence is linearly to the input fluence. Afterward as the input fluence increases, the output fluence does not increase linearly and finally is close to a constant. The optical limiting onset values F_{on}, defined as the

input fluence at which optical limiting activity starts, was tested about 0.16 J/cm^2. The above results show that the SnS_2 nanosheets display superior OL performance.

4. Conclusions

In conclusion，the NLO response of SnS_2 and $SnSe_2$ nanosheets is investigated using the Z-scan technique at 532 nm with nanosecond and picosecond laser pulses for the first time. SnS_2 nanosheets dispersions display RSA response at different pulse width. Meanwhile, both SnS_2 and $SnSe_2$ nanosheets firstly exhibit SA performance at a much low input energy caused by one-photon absorption and then change from SA to RSA by adjusting the input energy. The experimental results demonstrate that SnS_2 and $SnSe_2$ nanosheets have strong NLO absorption performance in the nanosecond and picosecond region. The figures of merit of SnS_2 and $SnSe_2$ nanosheet dispersions are 8.71×10^{-11} esu·cm and 11.98×10^{-11} esu·com at nanosecond pulse, respectively. However, at picosecond they decrease to 20.46×10^{-14} esu·cm and 3.63×10^{-14} esu·com, respectively. The nonlinear response in the nanosecond region seems to be much stronger than in picosecond regime. The strong NLO properties of SnS_2 and $SnSe_2$ nanosheets, along with their low cost and nontoxicity, make them potential candidates for optoelectronic application in optical limiters and optical switches.

Acknowledgements

We acknowledge the financial support from the National Science Foundations of China (No. 21673108 and 21573104), and the Open Foundations of State Key Laboratory of Coordination Chemistry (SKLCC1622).

References

[1] K. S. Novoselov, A. K. Geim, S. V. Morozov, D. Jiang, Y. Zhang, S. V. Dubonos, I. V. Grigorieva and A. A. Firsov, Science 306 (2004) 666–669.

[2] Y. R. Tao, X. C. Wu, W. Wang and J. N. Wang, J. Mater. Chem. C 3 (2015) 1347–1353.

[3] J. Kang, J. D. Wood, S. A. Wells, J. H. Lee, X. L. Liu, K. S. Chen and M. C. Hersam, ACS Nano 9 (2015) 3596–3604.

[4] G. K. Lim, Z. L. Chen, J. Clark, R. G. S. Goh, W. H. Ng, H. W. Tan, R. H. Friend, P. K. H. Ho and L. L. Chua, Nature photon. 5 (2011) 554–560.

[5] S. X. Wang, H. H. Yu, H. J. Zhang, A. Z. Wang, M. W. Zhao, Y. X. Chen, L. M. Mei and J. Y. Wang, Adv. Mater. 26 (2014) 3538–3544.

[6] F. Zhang, Z. X. Wu, Z. P. Wang, D. L. Wang, S. L. Wang and X. G. Xu, RSC Adv. 6 (2016) 20027–20033.

[7] D. Mao, B.B. Du, D. X. Yang, S. L. Zhang, Y. D. Wang, W. D. Zhang, X. Y. She, H. C. Cheng, H. B. Zeng and J. L. Zhao. Small 12 (2016) 1489–1497.

[8] K.G. Zhou, M. Zhao, M. J. Chang, Q. Wang, X. Z. Wu, Y.L. Song and H. L. Zhang. Small 11 (2015) 694–701.

[9] K.G. Zhou and H. L. Zhang. Small 11 (2015) 3206–3220.

[10] H. Zhang, S. B. Lu, J. Zheng, J. Du, S. C. Wen, D. Y. Tang and K. P. Loh, Opt. Express 22 (2014) 7249–7260.

[11] H. D. Xia, H. P. Li, C. Y. Lan, C. Li, J. B. Du, S. J. Zhang and Y. Liu, Photon. Res. 3 (2015) 92–96.

[12] K. Wu, X.Y. Zhang, J. Wang, X. Li and J. P. Chen, Opt. Express 23 (2015) 11453–11461.

[13] D. Li, H. Jussila, L. Karvonen, G. J. Ye, H. Lipsanen, X. H. Chen and Z. P. Sun. Sci. Rep. 5 (2015) 15899.

[14] S. B. Lu, L. L. Miao, Z. N. Guo, X. Qi, C. J. Zhao, H. Zhang, S. C. Wen, D. Y. Tang and D. Y. Fan. Opt.express 23 (2015) 11183–11194.

[15] Y. Sun, H. Cheng, S. Gao, Z. Sun, Q. Liu, F. Lei, T. Yao, J. He and S. Wei, Angew. Chem. Int. Ed. 51 (2012) 8727–8731.

[16] G. X. Su, V. G. Hadjiev, P. E. Loya, J. Zhang, S. D. Lei, S. Maharjan, P. Dong, P. M. Ajayan, J. Lou and H. B. Peng, Nano Lett. 15 (2015) 506–513.

[17] J. J. Wu, Y. R. Tao, Y. Wu and X. C. Wu, Sens. Actuators B 231(2016) 211–217.

[18] K. G. Liu, H. Liu, J. Y. Wang and L. M. Feng, Mater. Lett. 63 (2009) 512–514.

[19] A. J. Smith, P. E. Meek and W. Y. Liang, J. Phys. C 10 (1977) 1321–1333.

[20] H. S. Song, S. L. Li, L. Gao. Y. Xu, K. Ueno, J. Tang, Y. B. Cheng and K. Tsukagoshi, Nanoscale 5 (2013) 9666–9670.

[21] P. A. Fernandes, M. G. Sousa, P. M. P. Salomé, J. P. Leitão and A. F. da Cunha, CrystEngCommun. 15 (2013) 10278–10286.

[22] J. Camassel, M. Schlüter, S. Kohn, J. P. Voitchovsky, Y. R. Shen and M. L. Cohen, Phys. Stat. Sol. (b) 76 (1976) 303–314.

[23] J. Bordas, J. Robertson and A Jakobsson, J. Phys. C: Solid State Phys.11 (1978) 2607–2621.

[24] J. J. Wu, Y. R. Tao, J. N. Wang, Z. Y. Wu and L. Fan, Nanoscale 8 (2016) 10371–10379.

[25] M. Sheik-Bahae, A. A. SAID, T. H. WEI, D. J. Hagan and E. W. Van Stryland, *IEEE* J. Quantum Electron. 26 (1990) 760–769.

[26] N. Liaros, E. Koudoumas and S. Couris, Appl.Phys.Lett. 104 (2014) 191112.

[27] N. Liaros, K. Iliopoulos, M. M. Stylianakis, E. Koudoumas and S. Couris, Opt. Mater. 36 (2013) 112–117.

[28] S. F. Zhang, N. N. Dong, N. McEvoy, M. O'Brien, S. Winters, N. C. Berner, C. Y. Yim, Y. X. Li, X. Y. Zhang, Z. H. Chen, L. Zhang, G. S. Duesberg and J. Wang, ACS Nano 9 (2015) 7142–7150.

[29] S. Kumar, N. Kamaraju, K. S. Vasu, A. Nag, A. K. Sood and C. N. R. Rao, Chem. Phys. Lett. 499 (2010) 152.

[30] K. Wang, Y. Feng, C. Chang, J. Zhan, C. Wang, Q. Zhao, J. N. Coleman, L. Zhang, W. J. Blau and J. Wang, Nanoscale 6 (2014) 10530–10535.

[31] H. I. Elim, W. Ji, and M. T. Ng and J. J. Vittal, Appl. Phys. Lett. 90 (2007) 033106.

[32] H. I. Elim, J. Yang, J. Y. Lee, J. Mi and W. Ji, Appl. Phys. Lett. 88 (2006) 083107.

[33] N. N, Dong, Y. X, Li, Y. Y, Feng, S. F, Zhang, X. Y, Zhang, C. X, Chang, J. T, Fan, L. Zhang and J. Wang. Sci. Rep. 5 (2015) 14646.

Table 1. A comparison of SnS_2 and $SnSe_2$ dispersions with other NLO nanomaterials

Material	**Laser**	**α_0 (m^{-1})**	**NLO response**	**β (cm/GW)**	**Im$\chi^{(3)}$ (esu)**	**FOM×10^{-13} (esu·cm)**	**Ref**
$AgInSe_2$	200 fs 780 nm	610	SA	0.29	2.2×10^{-12}	3.6	30
Au	220 fs 800 nm	300	SA	1.5	1.2×10^{-12}	4	31
RGO	80 fs 395 nm	1.9×10^{6}	SA	25	7×10^{-12}	3.6×10^{-3}	28
WS_2	40 fs 800nm	1.08×10^{6}	TPA	(525±205)	$(2.7\pm0.8)\times10^{-9}$	$(2.5\pm0.8)\times10^{-2}$	25
MoS_2	100 ps532 nm	2570	SA	(26.2±8.8)	$(9.9\pm3.3)\times10^{-12}$	(3.8±1.3)	29
BP	30 ps 532 nm	585	TPA	16	5.14×10^{-12}	8.79	6
ZrS_3	6.5 ns 532 nm	62.48	RSA	44.2	13.8×10^{-12}	220.87	21
SnS_2	6.5 ns 532 nm	45.75	RSA	127.8	39.87×10^{-12}	871	This work
SnS_2	21 ps 532 nm	45.75	RSA	0.30	9.36×10^{-14}	2.05	This work
$SnSe_2$	6.5 ns 532 nm	32.75	SA	-125.8	-39.25×10^{-12}	1198	This work
$SnSe_2$	21 ps 532 nm	32.75	SA	3.8×10^{-2}	1.19×10^{-14}	0.36	This work

Figure Captions

Fig. 1 (a) XRD pattern of SnS_2 nanosheets; (b) XRD pattern of $SnSe_2$ nanosheets.

Fig. 2 (a) Low-magnification SEM image of SnS_2 nanasheets; (b) High-magnification SEM images of SnS_2 nanasheets; (c) Low-magnification SEM image of $SnSe_2$ nanasheets; (d) High-magnification SEM images of $SnSe_2$ nanasheets.

Fig. 3 (a) and (b)TEM image of SnS_2 nanosheets; (c) Selected area electron diffraction pattern of SnS_2; (d) HRTEM image of SnS_2 naaosheets;(e) Low-magnification TEM image of $SnSe_2$ nanosheets (f) TEM of individual $SnSe_2$ hexagonal sheets; (g) Selected area electron diffraction pattern; (h) HRTEM image of $SnSe_2$ nanosheets.

Fig. 4 (a) Raman spectrum of SnS_2 nanosheets; (b) Raman spectrum of $SnSe_2$ hexagonal nanosheets; (c) Absorption spectrum of SnS_2 nanosheets; (d) Absorption spectrum of $SnSe_2$ nanosheets.

Fig. 5 (a-d) Open-aperture Z-scan curves of SnS_2 dispersions in ethanol at different input energy; (e) Normalized transmittance versus input energy; (f) Fitting OA curves at different input energy; (g) β versus the input energy; (h) $Im\chi^{(3)}$ and FOM values versus the input energy.

Fig. 6 (a-b)OA Z-scan curves of $SnSe_2$ hexagonal nanosheets in ethanol dispersions at different input energy; (c) Fitting OA Z-scan curves normalized transmittance versus input energy; (d) Transmittance vs. input energy; (e) β versus the input energy; (f) $Im\chi^{(3)}$ and FOM values versus the input energy.

Fig. 7 OA curves in picosecond regime of (a) SnS_2 nanosheets and (b) $SnSe_2$ hexagonal nanosheets.

Fig. 8 Optical limiting of SnS_2 dispersions (a) normalized transmittance vs. input fluence; (b) output fluence vs. input fluence.

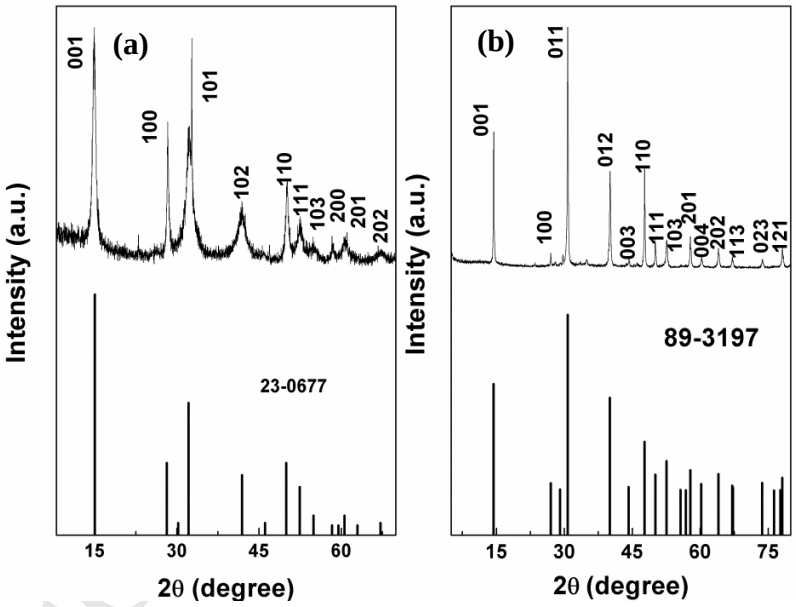
(a)
001
100
101
102
110
111
103
200
201
202
23-0677
Intensity (a.u.)
15
30
45
60
2θ (degree)
(b)
011
001
012
110
100
003
111
103
201
004
202
113
023
121
89-3197
Intensity (a.u.)
15
30
45
60
75
2θ (degree)

Fig. 1 Wu et al.

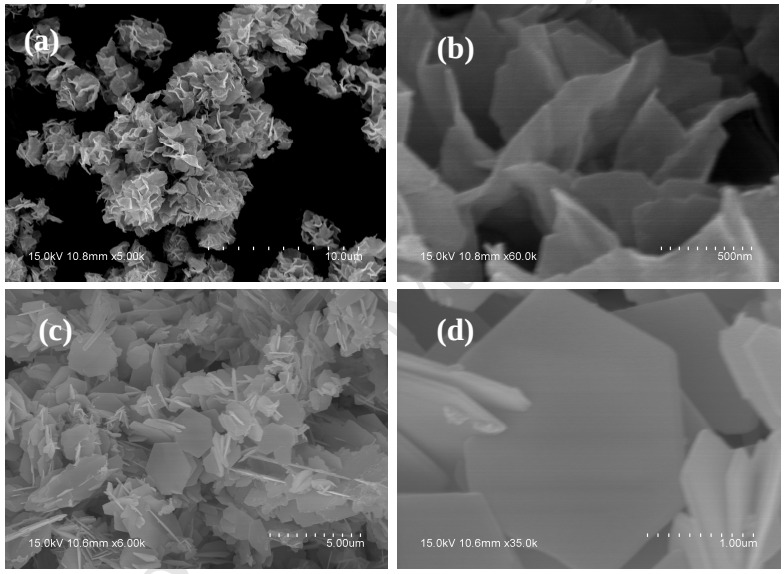
(a)
15.0kV 10.8mm x5.00k
10.0um
(b)
15.0kV 10.8mm x60.0k
500nm
(c)
15.0kV 10.6mm x6.00k
5.00um
(d)
15.0kV 10.6mm x35.0k
1.00um

Fig. 2 Wu et al.

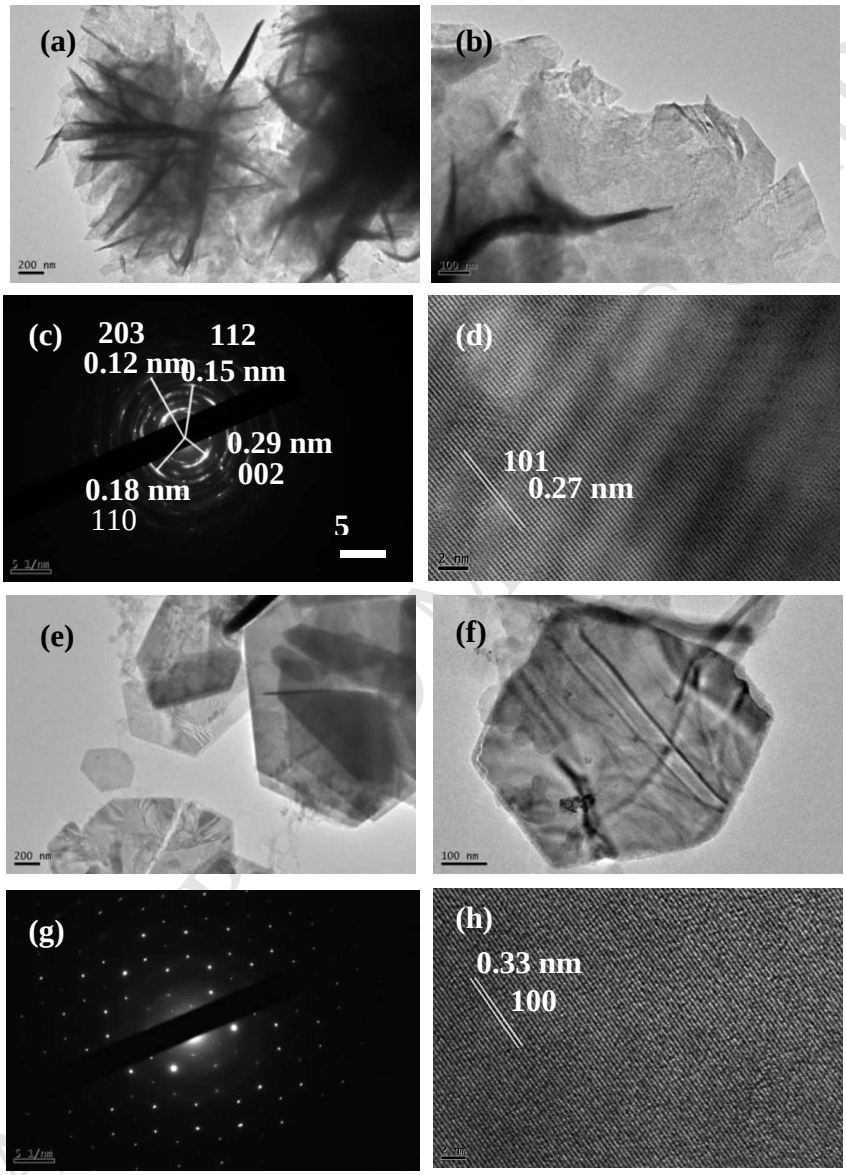
(a)
200 nm
(b)
100 nm
(c)
203
112
0.12 nm
0.15 nm
0.29 nm
002
0.18 nm
110
5
(d)
101
0.27 nm
2 nm
(e)
200 nm
(f)
100 nm
(g)
(h)
0.33 nm
100
2 nm

Fig. 3. Wu et al

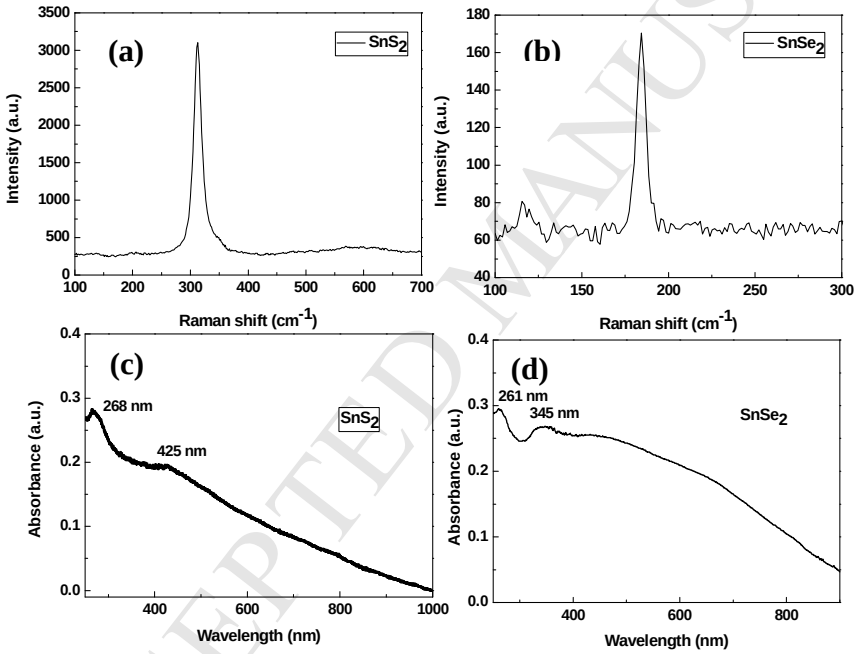

Fig. 4. Wu et al

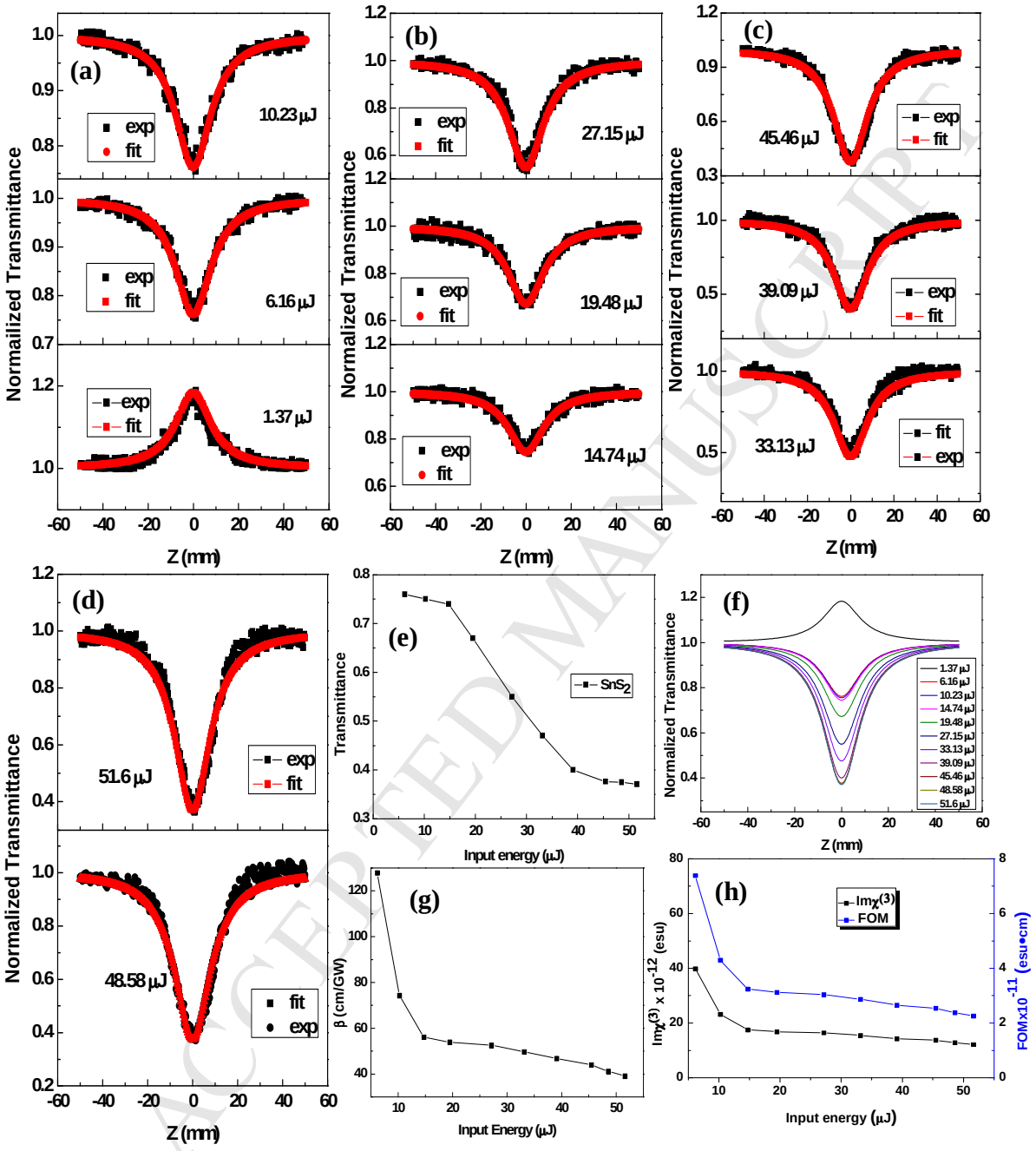
(a)
10.23 μJ
6.16 μJ
1.37 μJ
(b)
27.15 μJ
19.48 μJ
14.74 μJ
(c)
45.46 μJ
39.09 μJ
33.13 μJ
(d)
51.6 μJ
48.58 μJ
(e)
SnS2
Transmittance
Input energy (μJ)
(f)
Normalized Transmittance
Z (mm)
(g)
β (cm/GW)
Input Energy (μJ)
(h)
Imχ(3)
FOM
Imχ(3) x 10-12 (esu)
FOMx10-11 (esu•cm)
Input energy (μJ)
exp
fit
Normalized Transmittance
Z (mm)

Fig. 5. Wu et al

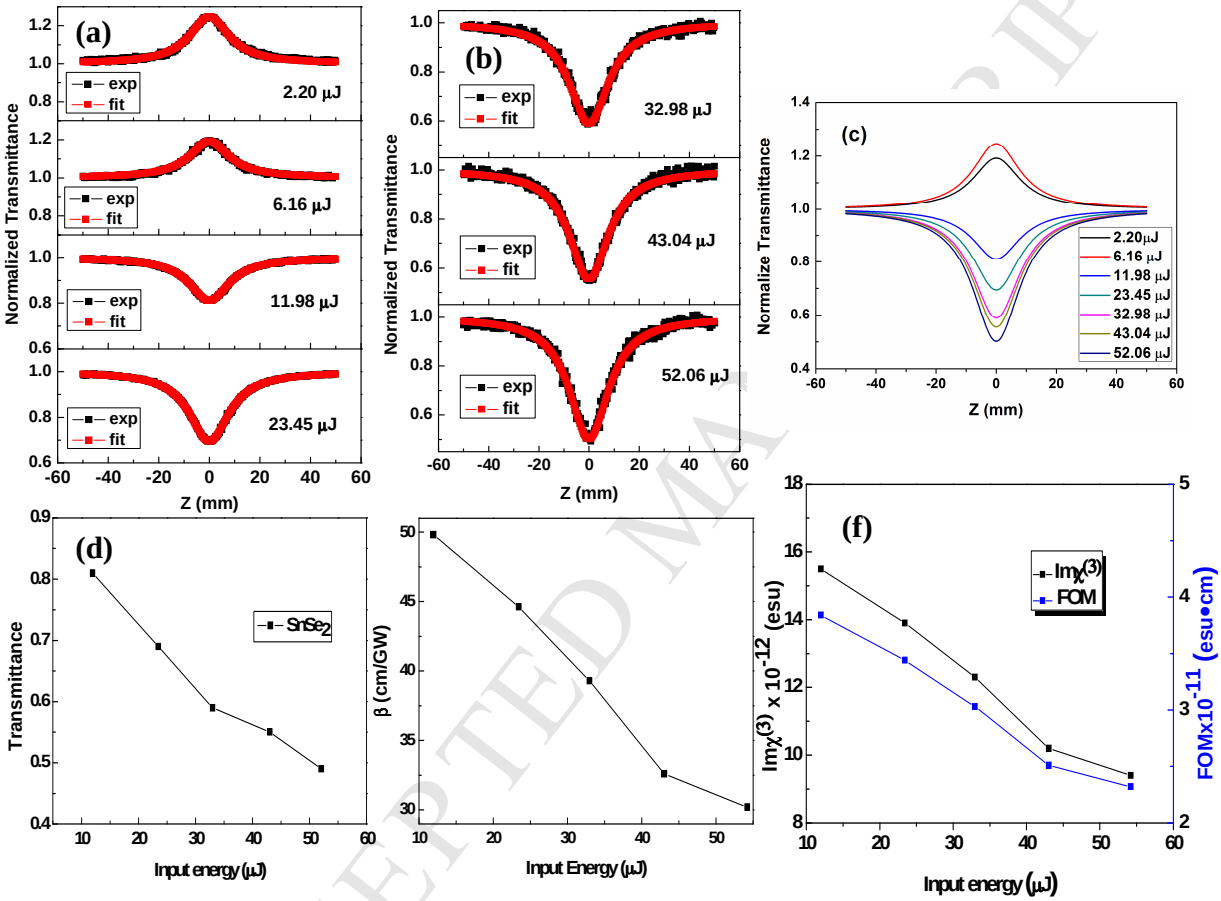
(a)
exp
fit
2.20 μJ
6.16 μJ
11.98 μJ
23.45 μJ
Normalized Transmittance
Z (mm)
(b)
32.98 μJ
43.04 μJ
52.06 μJ
(c)
Normalize Transmittance
2.20μJ
6.16 μJ
11.98 μJ
23.45 μJ
32.98 μJ
43.04 μJ
52.06 μJ
(d)
SnSe2
Transmittance
Input energy (μJ)
β (cm/GW)
Input Energy (μJ)
(f)
Imχ(3)
FOM
Imχ(3) x 10-12 (esu)
FOMx10-11 (esu•cm)
Input energy (μJ)

Fig. 6. Wu et al

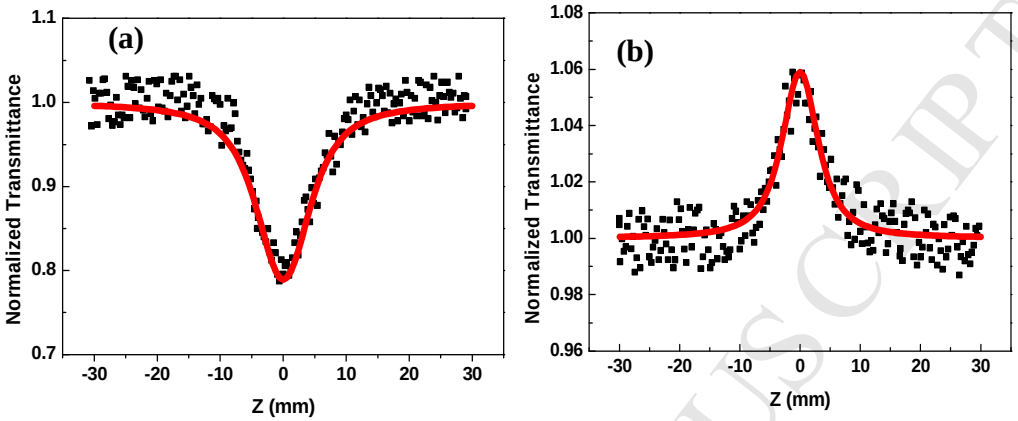

Fig. 7. Wu et al

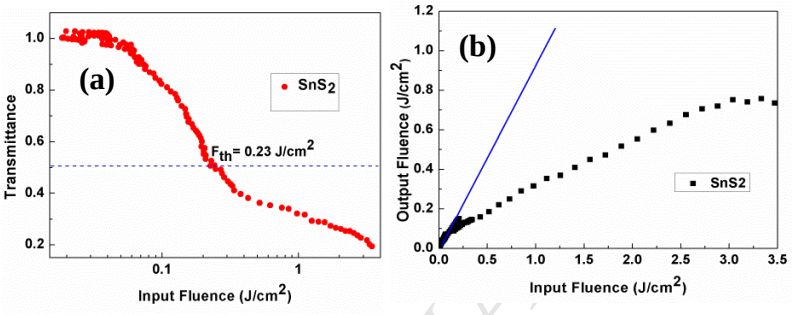

Fig. 8. Wu et al

Highlights

- We study the nonlinear absorption properties of SnS_2 and $SnSe_2$ for the first time.
- We find SnS_2 have excellent optical limiting for the first time.
- The optical limiting threshold F_{th} of SnS_2 is only about 0.23 J/cm^2.